Electronic structure, phase stability, equation of state, and pressure-dependent superconducting properties of Zr_3Al

P. Ravindran and R. Asokamani
Department of Physics, Anna University, Madras-600 025, India
(Received 18 January 1994)

We report here the ambient and high-pressure electronic-structure calculations of the potentially important ordered intermetallic alloy Zr_3Al obtained using the self-consistent linear muffin-tin orbitals (LMTO) method. Further total-energy calculations were made using the tight-binding LMTO scheme in the L_{12} and DO_{19} phases in order to study its structural stability. From total-energy studies and the band filling of bonding states results, we conclude that it is easier to create instability in the L_{12} lattice of Zr_3Al and this prediction is consistent with the experimentally observed martensitic structural transition from $DO_{19} \rightarrow L_{12}$ structure. To make a comparative study, the band structure and total-energy calculations of isoelectronic Ti_3Al were also made. The calculated bulk modulus and its pressure derivative, determined using a universal equation of state, are reported. The nature of chemical bonding in Zr_3Al is also discussed. Using the band-structure results, within the BCS formalism, the superconducting transition temperature (T_c) was calculated and it is compared with the experimental value. The ambient-pressure band-structure, and T_c calculations of the $A15$ compound Nb_3Al were made with a view to compare its superconducting behavior with that of Zr_3Al at high pressures as Zr_3Al should mimic Nb_3Al at high pressures. The pressure dependence of T_c of Zr_3Al is analyzed. Our calculations on Zr_3Al are in contradiction with the often quoted correlation between the low density of states at the Fermi level and structural stability in similar systems and this is further corroborated with our more recent studies on Ti_3In and Ni_3In.

I. INTRODUCTION

Studies on the intermetallic compound Zr_3Al are both of scientific and technological significance as it has attractive properties which make it useful for structural applications in thermal neutron reactors.[1-4] It has relatively simple crystal structure, which implies isotropic properties and potential toughness, and its specific thermal neutron-absorption capture cross section is only 0.96 m^2/m^3 compared to 17 m^2/m^3 in iron.[1] This compound has interesting mechanical properties, and some of them are the following: (i) The yield strength increases with increase of temperature.[2] (ii) Its work-hardening rate exceeds that of any fcc polycrystal, at least at low temperature.[3] (iii) Its ductility at ambient temperature is relatively large.

Even though the compound possesses the above said desirable properties, it swells ($\approx 1.5\%$ by volume) on irradiation and curiously it undergoes an embrittling crystalline-to-amorphous phase transformation when irradiated at temperature $\leq 400\,^{\circ}C$.[1,4] Irradiation-induced amorphization has been observed in semiconducting materials such as Si and Ge, but Zr_3Al also transforms from a crystalline to amorphous state when irradiated by energetic particles. At the same time, it is ductile at room temperature and below as in the case of metals. At least the ductility of Zr_3Al has been correlated with charge-density distributions using the results of a multiple-scattering $X\alpha$ cluster calculation.[5] Zr_3Al has been present in both cubic L_{12} and hexagonal DO_{19} structures[6] depending upon preparatory conditions. It is important to note that, compared to the hexagonal DO_{19} structure, the cubic L_{12} structure is more ductile.[7] Total energies which can be obtained from electronic-structure calculations have been used to study the structural stability of several systems, and the same procedure will be adopted for Zr_3Al. Hence, with the aim of gaining a better understanding of the structural stability and the mechanical properties of Zr_3Al, the electronic-structure studies of this material are essential and this motivated the present study.

In order to test the validity of the most recent equation of state which has been proposed by Vinet *et al.*, the universal equation of state (UEOS) is used to evaluate the bulk modulus and its pressure derivative from the calculated linear muffin-tin orbital (LMTO) pressures.[8] The band-structure calculations performed using the LMTO method were repeated using the tight-binding (TB) LMTO scheme also, as the latter is computationally more efficient for performing the total-energy calculations corresponding to different volumes. We expect a very small structural energy difference between the cubic and hexagonal structures because the differences in their atomic arrangements arise only from third-nearest neighbors onwards. The concept of electronegativity is made use of to explain the various factors such as the creation of what is called the pseudogap, structural stability, and chemical bonding.

With regard to the superconducting transition temperature, Wang *et al.* derived an analytical expression for calculating T_c from the atomic parameters for AB_3-type L_{12} superconductors.[9] From these studies they found

that in the case of L_{12} compounds, if the average atomic volume of the solid $V(L_{12})$ is less than that of the B constituent (V_B), they have strong electron-phonon coupling. Consequently, by applying external pressure, $V(L_{12})$ will decrease, and hence one can expect a higher T_c for L_{12} superconductors. In order to check the validity of this proposition, the superconducting behavior of Zr_3Al at high pressures was also studied. It has been observed experimentally that the superconducting behavior of Zr at high pressures is similar to that of Nb at ambient pressure.[10] In a similar way, one can expect the high-pressure superconducting behavior of Zr_3Al to be similar to the superconducting behavior of Nb_3Al at ambient pressure. So we made band-structure and T_c calculations of Nb_3Al at ambient pressure and compared them with high-pressure Zr_3Al.

This paper is presented in five sections. In Sec. II details with regard to the crystal-structural aspects of both cubic L_{12} and hexagonal DO_{19} structures along with the practical aspects of the linear muffin-tin orbital method are discussed. In Sec. III the electronic band structure and density of states (DOS) obtained from our calculations on both DO_{19} and L_{12} structures are presented. The pressure dependence of the DOS as well as the nature of the chemical bonding on Zr_3Al obtained from our band-structure calculations are also analyzed. In Sec. IV the results of the phase stability of Zr_3Al obtained from both DOS studies and total-energy calculations are presented. Further, the martensitic transformations from $DO_{19} \rightarrow L_{12}$ structures are also discussed. The bulk modulus and its pressure derivative obtained using the universal equation of state are presented in Sec. V. In Sec. VI the superconducting behavior of Zr_3Al as well as its variation with respect to pressure were studied and compared with the ambient pressure superconductivity observed in Nb_3Al.

II. CRYSTAL-STRUCTURAL ASPECTS AND METHOD OF CALCULATION

As mentioned earlier, Zr_3Al can crystallize either in the high-symmetry cubic L_{12} (Cu_3Au type) structure or in the hexagonal DO_{19} (Ni_3Sn type) structure.[6,11] In the cubic $CuAu_3$-type structure, each Al atom is surrounded by 12 Zr atoms as first-nearest neighbors and 6 Al atoms as second-nearest neighbors. A somewhat less symmetrical surrounding is found in the hexagonal DO_{19} structure, built up from the same close-packed AB_3 layers, where the number and distance of the neighboring Zr atoms and second-neighboring Al atoms are same as in the L_{12} structure as shown in Fig. 1(a). But two of the third-neighboring Al atoms are closer than in the Cu_3Au-type lattice and this will have a bearing on the total energies, however small they may be.

The energy-band structures were obtained by means of the linear muffin-tin orbital method within the atomic sphere approximation (ASA).[12,13] In all our calculations reported here, we assumed equal Wigner-Seitz (WS) radii for both transition metals and aluminum as the degree of overlap between the atoms lies within the allowed range,

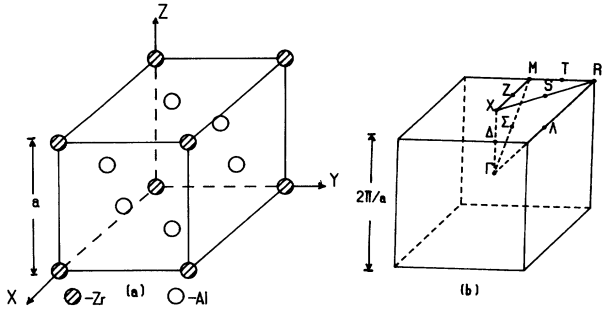

FIG. 1. (a) Unit cell of Zr_3Al simple cubic (L_{12}) crystal structure. (b) Symmetry labels for the first Brillouin zone of the simple cubic crystal lattice.

enabling the use of the LMTO ASA unlike the case with certain oxide compounds which we have studied earlier.[14,15] The average WS radius was scaled so that the total volume of all spheres is equal to the equilibrium volume of the primitive cell, and its values for all the systems we have studied are given in Table I. The Barth-Hedin exchange-correlation scheme is used in the construction of the potential.[16] The calculations are semirelativistic in nature where mass-velocity and Darwin terms are included in the solution of the Dirac equation, but with the spin-orbit terms excluded. We have included s, p, and d partial waves in the calculation, and the self-consistent iterations were carried out until an accuracy of 1 mRy was achieved in the eigenvalues. For all our calculations, we have used, respectively, 84 k points for the cubic L_{12} structure, 63 k points for the hexagonal DO_{19} structures, and 56 k points for the complex cubic $A15$ structure in the irreducible wedge of the first Brillouin zone (IBZ) for calculating eigenvalues. The c/a ratio of Zr_3Al in the DO_{19} structure is chosen in the same way as that of the isoelectronic compound Ti_3Al, and its value is 0.8006.[7] To study the phase stability of Zr_3Al and Ti_3Al, the electronic-structure studies and the total-energy calculations were made using the TB LMTO method at different reduced and extended volumes. The details of the TB LMTO calculations are found elsewhere.[17,18]

III. BAND STRUCTURE, DENSITY OF STATES, AND CHEMICAL BONDING OF Zr_3Al

A. Band structure

The band structure obtained for cubic Zr_3Al in $\frac{1}{48}$ of the first Brillouin zone [Fig. 1(b)] is given in Fig. 2. From the band structure, it is seen that the low-lying single band is mainly due to the Al s band and the cluster of nine bands present above this are contributing to the conduction states. These conduction bands are separated from the Al s band by an energy gap of 0.016 Ry, and the width of the conduction band (CB) is 0.356 Ry. The conduction bands are the hybridized bands of Zr s, Zr d, and Al p orbitals. The lower bands in the conduction state

TABLE I. Average Wigner-Seitz radius (R_{WS} in a.u.), the width of the occupied states, W_{occ} (Ry), the bonding states W_b (Ry), W_{occ}/W_b, and the number of the valence electrons to be accommodated in the bonding states (nb) for Zr_3Al and Ti_3Al in the L_{12} and DO_{19} structures. $N(E_{min})$ is the density of states (DOS) at the pseudogap, and $N(E_F)$ is the DOS at the Fermi level (in units of states/Ry f.u.). All these results are from LMTO calculations except those marked with a superscript a in last column.

Compound	R_{WS}	W_{occ}	W_b	W_{occ}/W_b	nb	$N(F_{min})$	$N(E_F)$	$N(E_F)$
$Zr_3Al(L_{12})$	3.230 191	−0.351	−0.328	1.070	13.97	13.12	41.04	36.25[a]
DO_{19}	3.230 191	−0.333	−0.344	0.970	15.12	11.74	15.87	18.47[a]
$Ti_3Al(L_{12})$	2.993 511	−0.380	−0.36	1.055	13.91	16.05	73.68	51.27[b]
DO_{19}	2.993 511	−0.366	−0.376	0.973	15.22	18.99	23.55	26.52[b]

[a]From the present TB LMTO calculation.
[b]$N(E_F)$ (states/Ry f.u.) from the LMTO results of Hong *et al.*

are mainly due to Zr s electrons, and above this a cluster of five bands is present, which are mainly contributed by Al p and Zr d orbitals. The bands which cross the Fermi level (E_F) are mainly the nonbonding states of the Zr d orbitals, and because of this, the major contribution to the density of states [$N(E_F)$] at the Fermi level is from Zr d electrons.

B. Density of states

The total and angular momenta decomposed density of states of Zr_3Al are shown in Figs. 3 and 4, respectively, and the dotted line indicates the Fermi level E_F. The DOS histogram of Zr_3Al obtained for the L_{12} structure consists of four parts: (i) The peak present in the lower-energy part of the DOS curve, which is mainly due to the localized or tightly bound s electron of Al, (ii) the sharp peak present around −0.17 Ry, which is mainly due to the hybridized bands of Al p with Zr d orbitals, (iii) the nonbonding states of Zr d orbitals near the Fermi level, and (iv) the top of the DOS curve due to antibonding states.

The peak in the lower-energy region of the DOS shown in Fig. 4 is due to Al s orbitals, which is clearly seen from the split DOS from Fig. 3. It is found that the Al s electrons in Zr_3Al are localized and naturally do not participate in bonding. The highest peak appearing in the DOS curve is due to the bonding states which arise from the hybridization of Al p and Zr d orbitals. The sharp peak in the DOS curve at E_F is mainly due to the nonbonding states of the Zr d electrons, and hence the physical properties of this compound should be mainly governed by Zr d electrons, which will be discussed later. Because of the sharp peak present in the vicinity of the Fermi level, the $N(E_F)$ value is large in Zr_3Al in the L_{12} structure. It is worth noting at this stage that this kind of peak at the Fermi level is exhibited by conventional high-T_c superconducting materials and ferromagnetic materials also.[19]

Because of the strong hybridization, a pseudogap, i.e., a deep valley close to E_F, is present around −0.044 Ry, and the DOS at this deep valley is 13.122 states Ry^{-1} $f.u.^{-1}$. Two mechanisms were proposed by Postural, Colinet, and Hicter for the formation of a pseudogap in binary alloys: One is of ionic origin, and the other is due to hybridization effects.[20] As the ionicity, i.e., the electronegativity difference, between Zr and Al is low, the pseudogap creation in Zr_3Al is not of ionic origin. The pseudogap present in Zr_3Al is found to be due to covalent hybridization between Zr and Al atoms as the valence states of the Al and Zr atoms have approximately the same energy. Such a strong hybridization gives not only

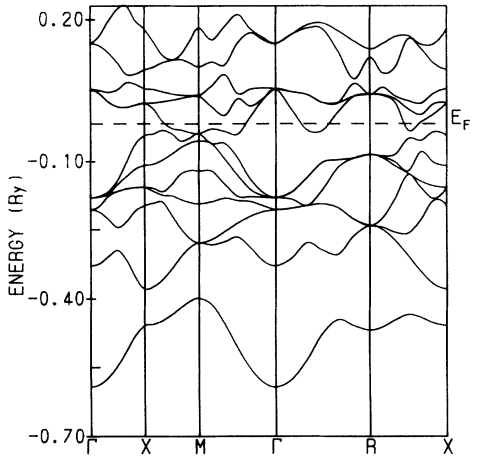

FIG. 2. Band structure of Zr_3Al.

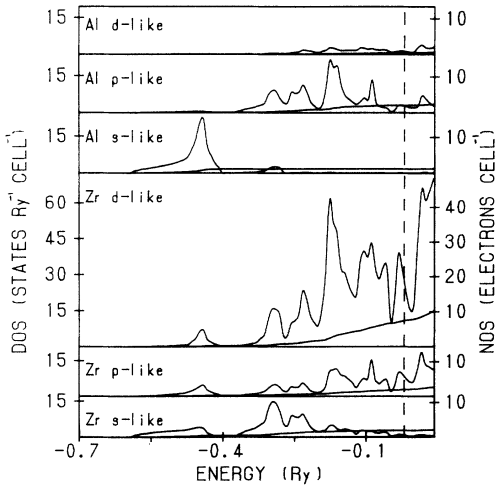

FIG. 3. Partial density of states of Zr and Al in Zr_3Al.

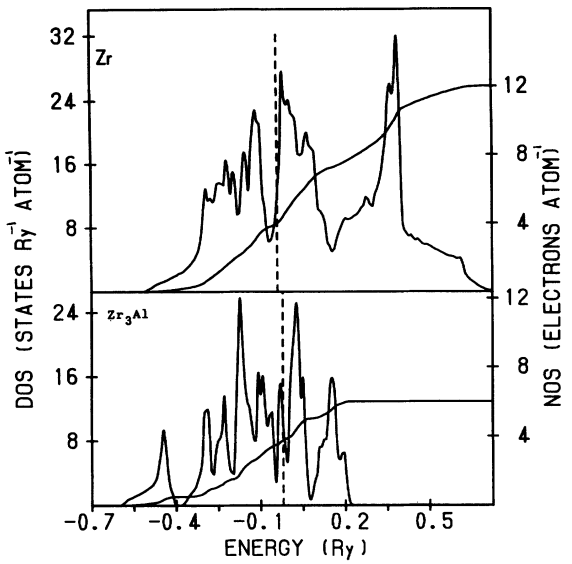

FIG. 4. Density of states of Zr_3Al and Zr.

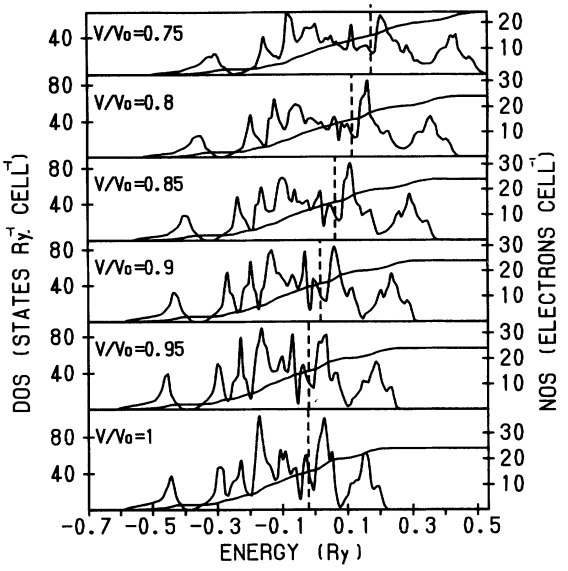

FIG. 5. Density of states of Zr_3Al at different V/V_0.

an important mixing between the states of the conduction bands, but also leads to a separation of the bonding states from the antibonding states, creating a pseudogap. It is interesting to note that the position of E_F is near the pseudogap in Zr_3Al (Fig. 4) as well as elemental Zr. This characteristic feature has been noted by Jepsen, Andersen, and Mackintosh in all hcp transition metals, and this is attributed to *d* resonance.[21] In the case of Zr_3Al, it is believed that both *p-d* hybridization and *d* resonance effects should be responsible for the creation of the pseudogap. The fact that the pseudogap may arise due to both factors as described above has been discussed in the case of TiB_2 also.[22]

C. DOS at high pressure in Zr_3Al

The pressure-dependent densities of state for Zr_3Al in the L_{12} structure for different compressed volumes are shown in Fig. 5. Because of the increasing electron concentration under pressure, the Fermi level gradually gets shifted to higher energies and the density of states at the Fermi level decreases with increase of pressure. The conduction bandwith becomes broader compared to the ambient pressure and does not contain sharp resonances, and all these features are in accordance with what one would normally expect.

D. Chemical bonding in Zr_3Al

The nature of the chemical bonding in transition-metal–non-transition-metal systems has been thoroughly studied through electronic-structure calculations.[23,24] From these studies, by analyzing the electronic density of states decomposed according to site and angular momenta, one can distinguish between ionic and covalent bondings in these systems. The bonding in Zr_3Al should be primarily of covalent nature as the valence states of the constituent atoms are approximately degenerate, which will lead a strong covalent hybridization as seen from Fig. 3. There are two factors which are responsible for the nature of the chemical bonding of Zr_3Al. The first one is the expansion of the Zr lattice due to the insertion of Al, and the second is the interaction between the valence *d* orbital of the transition metal Zr with the valence *p* orbital of Al. Comparison between the DOS curves of hcp Zr and cubic Zr_3Al (Fig. 4) shows that the conduction bandwidth of Zr_3Al is much less than that of Zr. It indicates that because of the expansion of the Zr lattice as mentioned above the intermetal bonding between Zr in Zr_3Al is weaker than that of hcp Zr.

Because of the strong *p-d* hybridization between Al and Zr, the melting point of Zr_3Al is more than that of its constituent Zr or Al metal. On account of the nature of the symmetry, not all the Zr *d* states are contributing to the *p-d* hybrid formation, and hence nonbonding states are present between the bonding and antibonding states (Figs. 3 and 4). Metallicity arising in Zr_3Al is due to this nonbonding state present at the Fermi level. But because of the covalent interaction between the Al *p* and Zr *d* electrons, Zr_3Al is not a good electrical conductor as has been observed experimentally.[25] As mentioned earlier, the ionic character in Zr_3Al is negligible due to the small electronegativity difference between Zr and Al. Hence Zr_3Al is a poor metal with covalent character.

IV. STRUCTURAL STABILITY

Some of the factors which decide the structural stability of AB_3-type compounds are the radius ratio, valence-electron concentration, the electronegativity of the atoms *A* and *B*, and the addition of substitutional or interstitial impurities.[26] It is found that most of the stable cubic L_{12}-type AB_3 compounds have a radius ratio (r_A/r_B) in the vicinity $0.7331-1.331$.[27] They are more stable when $r_A/r_B \approx 1$, and deviation from this value leads to hexagonality.[28] The atomic radii of Zr and Al in Zr_3Al are 0.167 and 0.1338 nm, respectively, in the L_{12} structure.[27]

Since the radius ratio deviates from the ideal value of 1:1.251, this is bound to have a greater influence on the crystal-structural stability. The electronegativity difference between Zr and Al being only 0.1, its influence on structural stability can be neglected.

A strong correlation has been often emphasized between the position of the pseudogap and structural stability. It has been demonstrated both experimentally and theoretically that the material is found to be more stable in that particular structure if the filling of the bonding states is maximum. For most stable structures, there is enough room to accommodate all its valence electrons into the bonding states so as to bring the Fermi level to the pseudogap. In other words, the stable structure is often characterized by a low $N(E_F)$.[29–32]

The essential contribution to the cohesion of Zr_3Al is the hybridization between the Zr d and Al p states. Filling bonding states will increase the cohesion, and filling antibonding states will decrease cohesion.[33] Similarly, we expect that the phase stability will depend upon the band filling of bonding states. In order to understand the correlation between the structural stability and the filling of the bonding states in the two structures (L_{12} and DO_{19}), the related parameters for both Zr_3Al as well as Ti_3Al are given in Table I and the corresponding DOS curves are shown in Fig. 6. Here we denote the width of the occupied state by W_{occ} and the width of the bonding states by W_b, which are the energy differences from the bottom of the conduction band to E_F and the valley, respectively. The ratio W_{occ}/W_b is used to evaluate the occupied portion of the bonding states, i.e., the band filling of the bonding states. We can clearly see from Table I that the stable phase for Ti_3Al (DO_{19}) is always the one having the maximum of the bonding states, as has been observed in earlier studies.[7] The overall topology of the DOS curve of Ti_3Al in the L_{12} and DO_{19} structures is almost similar to that of previous studies. The DOS curve of Ti_3Al in Fig. 6 clearly shows that the stable DO_{19} structure is having more $N(E_F)$ than the L_{12} structure. From Table I, it is also seen that the $W_{occ}/W_b \approx 1$ for hexagonal Zr_3Al compared to the cubic one, and correspondingly $N(E_F)$ for the hexagonal structure is less than the cubic structure, as shown in Fig. 6. These results lead one to expect hexagonal Zr_3Al to be more stable than cubic Zr_3Al, which is contrary to experimental observations.[6,11]

For cubic Zr_3Al, the ratio of W_{occ}/W_b (1.084) is slightly larger than 1, which means that the bonding states of cubic Zr_3Al already have no room for accommodating all its conduction electrons. Our calculations show that only 11.927 valence electrons can be accommodated in its bonding states. Hence the remaining 1.073 electrons must go into the high-energy region, i.e., in the nonbonding states. From Table I, it is observed that from the degree of band filling of the bonding states, the metastable DO_{19} structure Zr_3Al is more stable against the experimentally observed stable L_{12} structure. So in Zr_3Al the phase stability analysis in terms of the band filling of bonding states does not hold good in predicting the stable structure. Further, our band-structure and total-energy studies performed on Ti_3In and Ni_3In also lend strong support to the above viewpoint.[34] Hence it seems that the low density of states at the Fermi level is not always a necessary condition to predict the stable structure. These observations are also supported by the experimental phase stability studies made by Kuentzler and Waterstrat.[19]

So far we have tried to analyze the structural stability of Zr_3Al from its density-of-states results. Now we proceed to calculate its total energy in the cubic L_{12} and hexagonal DO_{19} structures both for compressed and expanded lattices to look for its minimum energy. Total energies were calculated using the TB LMTO scheme, and the results obtained are shown in Fig. 7. It is obvious from Fig. 7 that the L_{12} structure is more stable compared to the DO_{19} structure, in agreement with experimental observations. However, it should be noted that the minimum energy does not correspond to $V/V_0=1$ and this is due to the use of the local-density approxima-

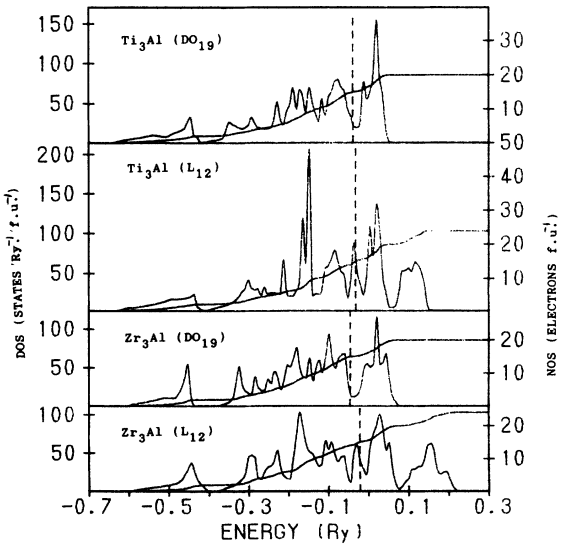

FIG. 6. Density of states of Zr_3Al and Ti_3Al in the L_{12} and DO_{19} structures.

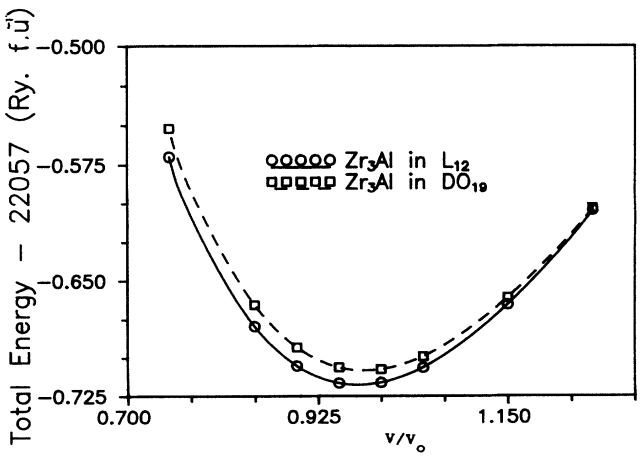

FIG. 7. Total energy as a function of volume in Zr_3Al in the L_{12}- and DO_{19}-type structures.

tion as has been observed in all the calculations. The contradicting results obtained from the DOS results and the total-energy calculations will be discussed in detail in a later section.

In Zr_3Al the density of states at the Fermi level falls on a sharp peak, indicating that it is less stable. The above result makes us predict the $DO_{19} \rightarrow L_{12}$ martensitic transformation which has been experimentally observed. Further, because of the large density of states at the Fermi level, one can expect a large value of paramagnetic susceptibility which will be varying with the applied field as has been observed in some of the L_{12} superconductors.[35] But no such experimental study has been made for this compound so far. Structural instabilities in transition-metal compounds are often associated with the superconducting property. It is interesting to note that the values of the electronic specific-heat coefficient γ and the superconducting transition temperatures are related to the martensitic transformation temperature T_m,[36,37] i.e., high $N(E_F)$, and hence T_c corresponds to a low T_m value. It is inferred that due to the possibility of the martensitic transformation taking place at high temperature or due to the metastable phase, the minimum $N(E_F)$ is not reached in Zr_3Al in its L_{12} structure, and a similar situation has also been observed in the binary systems ZrRh, HfRh, and TiRh.[19,32]

V. EQUATION OF STATES STUDIES FOR Zr_3Al

Vinet *et al.* have proposed a universal equation of state which will be valid for all classes of solids under compression.[8] According to them, if one defines x as $(V/V_0)^{1/3}$ and $H(x)=x^2P(x)/3(1-x)$, then the $\ln[H(x)]$ versus $1-x$ curve should be nearly linear and obey the relation

$$\ln[H(x)] \approx \ln B_0 + \eta(1-x) . \quad (1)$$

The isothermal EOS is expressed as

$$P=[3B_0(1-x)/x^2]\exp[\eta(1-x)] . \quad (2)$$

The slope of the curve (η) is related to the pressure derivative of the bulk modulus (B_0') by

$$\eta=\tfrac{3}{2}[B_0'-1] . \quad (3)$$

The LMTO results along with the frozen potential approximation were used to obtain the pressure for the specified cell volume chosen in terms of the moment of the projected state densities. The calculated values of the pressure at different cell volumes for cubic Zr_3Al are plotted in Fig. 8. In order to test the applicability of the UEOS for Zr_3Al, we calculated the values of $\ln[H(x)]$ and $1-x$ using the P-V data and made the least-squares fit. This fitted curve, shown in Fig. 9, exhibits excellent linearity as anticipated, and the intercept of the curve gives $\ln(B_0)$. From this, the calculated bulk modulus of Zr_3Al is found to be 0.870 Mbar and it is comparable with the value of the bulk modulus of Zr, which is 0.849 Mbar.[38] The pressure derivative of the bulk modulus (B_0') calculated from the expression for η was found to be 4.766. From the theoretically obtained P-V curve (Fig. 8), the equilibrium volume is estimated and the corresponding equilibrium lattice constant is 4.566 Å, which differs by 4.395% from the experimental value. It should be noted that this much deviation in the lattice parameter has been observed in the case of TiB_2 in the recent calculations performed using the LMTO method,[22] and it is satisfying to note that the present calculation has been able to predict a fairly accurate equilibrium lattice constant.

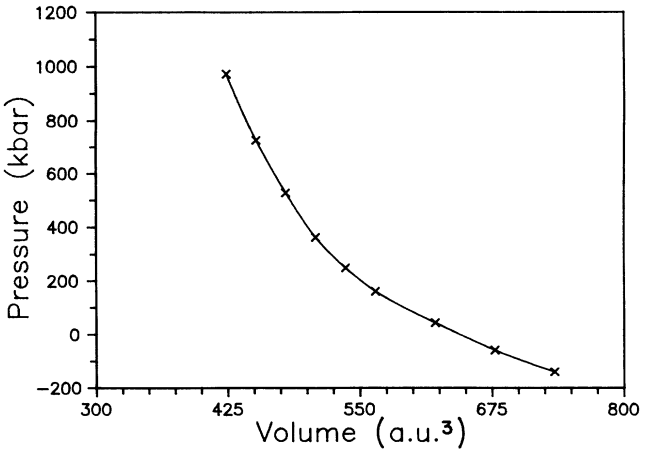

FIG. 8. EOS of Zr_3Al.

VI. SUPERCONDUCTIVITY IN Zr_3Al

Zr_3Al is a superconductor with a T_c of 0.73 K in which zirconium is considered to be the more decisive element in determining the occurrence of superconductivity. In the L_{12}-type superconducting compounds, a correlation between the T_c and the atomic parameters has been observed, and from this correlation the T_c of Zr_3Al has been predicted to be 1.3 K.[9] In the present work, we have used the McMillan's formula[39] to determine the superconducting transition temperature and its variation with pressure using the band-structure results.

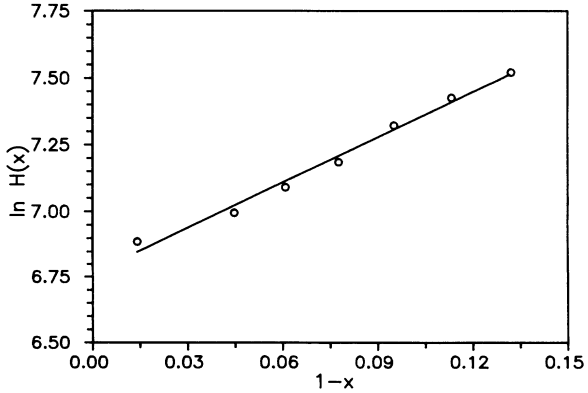

FIG. 9. Calculated $\ln H(x)$ vs $1-x$ curve for Zr_3Al: calculated result (○) and best-fit line.

A. Calculation of the electron-phonon coupling constant (λ) and T_c

One of the important applications of the electronic-structure calculations is the determination of the electron-phonon coupling constant, which in turn can be used to estimate the superconducting transition temperature. A detailed discussion of the evaluation of λ and T_c may be found elsewhere.[40] However, for the sake of completeness, we describe here briefly the method adopted for the calculation of λ and T_c. Using the McMillan formula, we have calculated the T_c value, which is written as[39]

$$T_c=\frac{\theta_D}{1.45}\exp\left\{\frac{-1.04(1+\lambda)}{\lambda-\mu^*(1+0.62\lambda)}\right\}, \tag{4}$$

where θ_D is the Debye temperature and λ and μ^* are, respectively, the electron phonon (e-p) coupling constant and the electron-electron interaction parameter. The electron-phonon coupling constant was evaluated using the formula

$$\lambda=N(E_F)\langle I^2\rangle/M\langle\omega^2\rangle\ , \tag{5}$$

where M is the atomic mass, $\langle\omega^2\rangle$ is an average-squared phonon frequency, and $\langle I^2\rangle$ is the square of the electron-phonon matrix element averaged over the Fermi surface. In the atomic sphere approximation, $\langle I^2\rangle$ can be written as[41]

$$\langle I^2\rangle=2\sum_l \frac{(l+1)}{(2l+1)(2l+3)}\underline{M}^2_{l,l+1}\frac{N_l(E_F)N_{l+1}(E_F)}{N(E_F)N(E_F)}, \tag{6}$$

where $\underline{M}_{l,l+1}$ is the electron-phonon matrix element. The necessary parameters to calculate $\underline{M}_{l,l+1}$ are taken from the band-structure results. In the case of compounds, λ may be split as

$$\lambda=\sum_i\lambda_i\ , \tag{7}$$

where the summation runs over all the atoms in the primitive cell. The value of 0.13 is used for μ^*, which is commonly used for transition metals. The average squared of the phonon frequency $\langle\omega^2\rangle$ which appears in Eq. (5) is set equal to $0.5\theta_D^2$.[42] In the cases of transition-metal aluminides, as the mass difference between the constituent atoms is large, the respective $\langle\omega^2\rangle$ values of transition metals and Al were obtained from the above relation by substituting the corresponding Debye temperature of the elemental transition metal[43] and Al as has been done earlier.[44] The average squared of the phonon frequency will be really sensitive to both temperature and pressure. But very limited information concerning the analogous changes in the phonon spectrum at high pressure is available.[45] Because of the nonavailability of the phonon spectrum of Zr_3Al at high pressure, we assumed the ambient-pressure Debye temperature at high pressure also. The calculated value of electron-phonon coupling constant using Eq. (5), the T_c value calculated using Eq. (4), and other parameters involved in the T_c calculations are given in Table II. In view of the different approximations used in the calculation of T_c, it is satisfactory to note that the calculated values of T_c are closer to the experimental values.

VII. RESULTS AND DISCUSSION

As far as the band-structure results are concerned, it can be seen from Fig. 2 that the s band arising from the Al atom lies deeper, indicating that the s electrons of Al are localized. This is also reflected in the corresponding density-of-states histograms (Figs. 3 and 4). Insertion of Al atoms has weakened the d-d interaction between Zr atoms, and because of the localization of the s electrons of Al, the conduction bandwidth of Zr_3Al has been decreased compared to elemental Zr (Fig. 4). Correspondingly, the DOS at the Fermi level is larger than that of Zr. In the case of cubic Zr_3Al, the Al-Al distances are greater than those between Zr-Al as well as Zr-Zr [Fig. 1(a)], and hence Zr-Zr and Zr-Al interactions are more

TABLE II. Parameters related to the T_c calculation of Zr_3Al as a function of V/V_0 and Nb_3Al: electronic density of states at the Fermi level, $N(E_F)$ [states/Ry f.u.], the electronic contributions arising from the transition-metal (TM) and Al sites, and η_{TM} and η_{Al} (eV/A^2); electron-phonon interactions from the TM and Al sites, λ_{TM} and λ_{Al}, calculated and measured T_c (K). The above parameters for Zr_3Al at ambient pressure and high pressures (in the L_{12} structure) and the DO_{19} structure at ambient pressure are given. Present theoretical results along with the other theoretical and experimental results for Nb_3Al in the $A15$ structure are also given.

V/V_0	$N(E_F)$	η_{Zr}	η_{Al}	λ_{Zr}	λ_{Al}	η	λ	T_C Theory	T_C expt.
1.0	41.04	2.458	0.023	0.485	0.006	2.481	0.49	1.40	0.73
0.9	28.98	2.521	0.014	0.498	0.004	2.536	0.50	1.55	
0.85	26.70	2.888	0.011	0.570	0.003	2.899	0.57	2.80	
0.8	24.31	3.269	0.009	0.645	0.002	3.279	0.64	4.36	
0.75	23.88	4.068	0.011	0.803	0.003	4.080	0.81	7.99	
Zr_3Al (DO_{19})	15.87	0.678	0.008	0.133	0.002	0.686	0.135	0.00	
Nb_3Al (A15) $R_{WS}=3.040\,341$ a.u.	77.14	4.197	0.040	0.875	0.009	4.23	0.885	14.50	18.6
a	99.6	13.40	0.05			13.45	2.14	25.1	
b	76.89					6.20	1.07	18.65	

[a]Reference 50.
[b]Reference 58.

dominant than the Al-Al interaction. The DOS histogram due to Al s electrons in Zr_3Al looks the same as that in Zr_2Al, and charge density distribution studies on Zr_2Al show that the valence band arises from Al s electrons.[46] The DOS of Zr_3Al is almost similar to that of hcp Zr except for the finer oscillations, which are due to the hybridization of Zr with Al. As suggested by Gelatt, Williams, and Moruzzi,[24], filling nonbonding states has little effect on the bondstrength of diatomic molecules (systems of AB type), but in Zr_3Al these states in fact contribute to the Zr-Zr intermetal bonding. This bonding becomes weaker due to the increase of the Zr atom separation by the accommodation of the aluminum and hence the d-band width decreases (Fig. 4).

A strong correlation has often been emphasized between structural stability and the density of states at the Fermi energy $[N(E_F)]$.[29–32] It has also been observed in a number of A_3B systems that the system crystallizes in that structure for which $N(E_F)$ is minimum. But on the contrary, our band-structure results show that the stable L_{12} structure has large $N(E_F)$ compared to the metastable DO_{19} structure. To settle the issue, total-energy calculations were performed using the tight-binding LMTO scheme. The $N(E_F)$ calculated from TB LMTO's is found to be in good agreement with the LMTO ASA results (Table I). The total-energy curves obtained for Zr_3Al for L_{12} and DO_{19} structures are given in Fig. 7. As stated earlier, differences in the arrangement of atoms between the above structures begin only from third-nearest neighbors onwards and one can anticipate only small energy differences between these two structures. Our total-energy calculations clearly show that the L_{12} structure is more favored compared to the DO_{19} structure, which is in agreement with the experimental observation. The total-energy curves further show that at extended volumes the total energies of both L_{12} and DO_{19} structures are almost the same, and this probably indicates the possibility of a martensitic transformation from the $DO_{19} \rightarrow L_{12}$ structure, which has been observed experimentally.[47] In Zr_3Al in the L_{12} structure the Fermi level falls on the nonbonding region of the DOS curve, and because of this, instability arises. Similarly to Zr_3Al in $ZrAl_3$, also, the Fermi level falls on the nonbonding region, and this led Xu and Freeman to find the cause of metastability in the latter.[48]

In order to verify the validity of the above said correlation, band-structure and total-energy calculations were performed in Ti_3X and Ni_3X (X=Al, Ga, In) for both L_{12} and DO_{19} structures.[34] The DOS obtained for Ti_3Al shown in Fig. 6 is very much similar to those obtained earlier by LMTO and FLAPW results.[7] Ti_3Al has a low $N(E_F)$ for the stable DO_{19} structure, and the same structure is favored by total-energy calculations also. On the other hand, the contradictions as observed in Zr_3Al are also observed in Ti_3In and Ni_3In.[34] These results have led us to conclude that low $N(E_F)$ is not a necessary condition for structural stability. One should rely on total-energy calculations for structural stability instead of the position of E_F in the DOS curve.

As mentioned earlier, the bonding in Zr_3Al is definitely not ionic and its electrical resistivity is $49.3\times10^{-6}\Omega$ cm, which shows that it is a poor metal.[25] No Fermi-surface study has been made on this compound, and more recently such a study has been made on the isostructural system Ni_3Al.[49] As discussed earlier, there is a strong covalent hybridization in this system, which indicates that the bonding is indeed a mixed one, arising out of covalent and metallic characters.

Using the LMTO method, the UEOS of TiB_2 has been successfully studied recently.[22] Pressure studies have been made use of to extract the numerical values of the bulk modulus (B_0) and its pressure derivative (B_0') using the UEOS. The value of the isothermal bulk modulus for Zr_3Al is 0.87 Mbar as against 1.2 Mbar for the isoelectronic compound Ti_3Al[7]. These values, when compared with the values of elemental Zr and Ti, which are 0.8496 and 1.072 Mbar, respectively, indicate the greater role played by the A atoms in these A_3B-type compounds with respect to mechanical properties such as compressibility.

Apart from the study of compressibility, the other quantities which were determined are the electronic specific-heat coefficient (γ), the Pauli paramagnetic susceptibility (χ_P), and the superconducting transition temperature (T_c), which directly depend upon $N(E_F)$. Using the value of $N(E_F)$ calculated for the L_{12} structure in which Zr_3Al normally crystallizes, the values of γ and χ_P were found to 7.1349 mJ/mol K^2 and 9.766×10^{-5} emu/mol, respectively. As the Fermi level of Zr_3Al falls on a sharp peak in the DOS curve, we expect a considerable variation in χ_P and γ with temperature as was observed in the L_{12} superconductors La_3In and La_3Tl from NMR studies[35] as well as the $A15$ compound Nb_3Sn.[50] But no such experimental studies are available for Zr_3Al to confirm our expectation.

We determined the value of T_c at ambient pressure using the band-structure results in McMillan's relation as has been done previously.[44] As the Debye temperature of Zr_3Al was not available, we used the θ_D value of Zr.[43] Since the bulk modulus of Zr_3Al is not much different from Zr, as has been seen earlier, the differences in their lattice stiffness or Debye temperatures should be small. From ambient-pressure T_c calculations, we found that the electronic contribution (η_{Zr}) arising from Zr was important to determine the superconducting behavior of Zr_3Al (Table II). It is strongly believed that the d-electron number and d density of states are the prime factors to decide superconductivity in transition-metal compounds. It has been experimentally observed that the T_c value of hcp Zr was found to increase with increase of pressure, and it was concluded that because of $s \rightarrow d$ electron transfer at high pressure, Zr will behave like Nb at high pressure.[10] Because of the dominance of Zr d electrons in the superconducting behavior of Zr_3Al, we can expect this compound also will show an increasing trend in T_c with pressure. In order to understand the pressure dependence of T_c in Zr_3Al, we made systematic band-structure studies on it at different reduced volumes up to $V/V_0=0.75$. From the high-pressure band-structure results in Table III, it is found that the d-electron number

TABLE III. Density of states at the Fermi energy $N(E_F)$ (states/Ry f.u.), partial number of states (electrons/atom) split by angular momentum, and site of Zr_3Al in the L_{12} structure at different reduced cell volumes. Note that the Zr d electron increases from 7.467 to 8.301, which shows $s,p \rightarrow d$ electron transfer.

V/V_0	$N(E_F)$	N^s_{Zr}	N^p_{Zr}	N^d_{Zr}	N^s_{Al}	N^p_{Al}	N^d_{Al}
1.0	41.042	1.936	1.923	7.467	1.219	2.043	0.409
0.95	32.606	2.043	2.276	7.822	1.099	1.547	0.211
0.90	28.982	2.008	2.223	7.912	1.085	1.552	0.218
0.85	26.707	1.966	2.160	8.019	1.071	1.555	0.226
0.80	24.707	1.966	2.915	8.149	1.058	1.555	0.235
0.75	23.882	1.859	2.000	8.301	1.045	1.548	0.244

increases as a function of pressure. It is well known that $s \rightarrow d$ electron transfer is one of the chief mechanisms responsible for promoting superconductivity in solids under pressure. Theoretical electronic-structure calculations as well as optical-reflectivity experiments under pressure offer evidence in support of $s \rightarrow d$ electron transfer in solids.[51–53] The calculated T_c values and other important parameters involved in the T_c calculations are given in Table II. From the pressure dependence of the T_c calculation of Zr_3Al, we found that, like hcp zirconium, the T_c value of Zr_3Al rose from 1.40 to 7.99 K until V/V_0 was reduced to 0.75, as we expected.

From the increasing trend in T_c with pressure in Zr_3Al and the increasing d-electron number with pressure due to $s \rightarrow d$ electron transfer, one can expect that the superconducting behavior of Zr_3Al at high pressure is similar to that of Nb_3Al at ambient pressure. In order to compare the superconducting behavior of high-pressure Zr_3Al with that of ambient-pressure Nb_3Al, we made normal-pressure band-structure studies and T_c calculations on Nb_3Al. The calculated results are compared with previous theoretical and experimental studies, and these are tabulated (Table II). From our calculations we found that the main cause for a large T_c in Nb_3Al is due to the large density of states at the Fermi level. But in Zr_3Al, $N(E_F)$ gradually decreases with increase of pressure, as it ought to be. The above-mentioned differences between their density of states are clearly brought out in Fig. 10. In general, transition-metal superconducting compounds having large $N(E_F)$ possess large T_c. But the $N(E_F)$ effect is not very much important to promote superconductivity in Zr_3Al at high pressures. From his theoretical studies, Butler concluded that the materials which have a strong hybridization have a large T_c compared to weakly hybridized solids.[54] So the $s,p \rightarrow d$ electron transfer and the strong hybridization at high pressures are the prime factors for promoting superconductivity in Zr_3Al apart from the phonon part. In this case, the increase in T_c is mainly due to increase in d-electron number, as seen in Table II (which is by about one electron), and this arises because of $s,p \rightarrow d$ electron transfer.

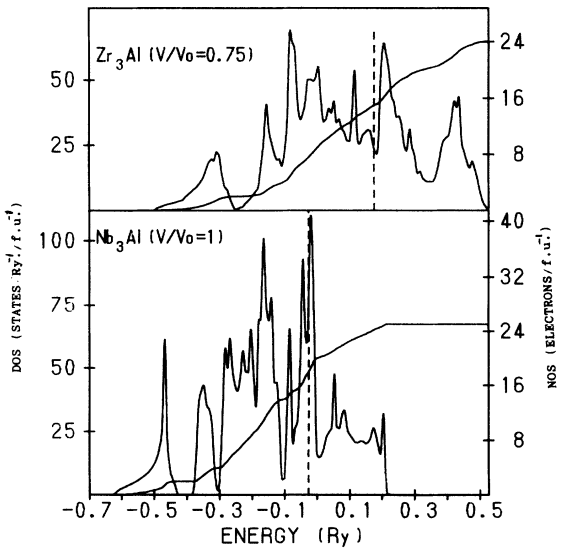

FIG. 10. Density of states of Nb_3Al and Zr_3Al ($V/V_0=0.75$).

At high pressures $\langle\omega^2\rangle$ is bound to increase unless there is a structural transition. The variation of $\langle\omega^2\rangle$ with pressure has not been taken into account in this calculation even though an attempt has been made by us with respect to elements.[40,55] It should be noted that structure also plays an important role in controlling T_c. The value of T_c calculated for Zr_3Al in the hexagonal DO_{19} phase was found to be almost zero. The fact that T_c is sensitive to the structure has been brought out from some of the earlier calculations.[56,57] As mentioned before, one can correlate the T_c of L_{12} superconductors with the ratio of V_B and V_{L12}, where V_B and V_{L12} are atomic volumes in the pure B and in the L_{12} compound, respectively.[9,27] From the correlation it was observed that if the V_B/V_{L12} ratio is large, the compound will have large T_c. The superconductivity studies we have made on Zr_3Al under high pressure using our band-structure results support the above viewpoint.

VIII. CONCLUSION

The important conclusions arrived at from the above work on the potentially important nuclear engineering material are as follows.

(i) The correlation which has been quoted often connecting low $N(E_F)$ and structural stability in AB_3 or A_3B compounds need not work always as has been the case with Zr_3Al. There are certain other systems such as

Ti_3In and Ni_3In which yield results similar to that of Zr_3Al. However, total-energy calculations correctly predict the structure, and more than that, they are able to predict also the martensitic transformation which has been observed experimentally. It seems that the above-mentioned correlation will not work in systems which are in the metastable state.

(ii) Apart from the creation of a pseudogap in Zr_3Al similar to the case of elemental Zr, it is interesting to find that many other physical properties show strikingly similar behavior. For instance, the values of the bulk modulus, electrical resistivity, and even the superconducting transition temperature of Zr_3Al are similar to that of Zr. In addition, the trends in the variation of T_c with pressure in Zr_3Al and Zr remain the same.

(iii) The large T_c value in Nb_3Al is due to the large value of $N(E_F)$. In Zr_3Al, instead of the DOS effect, the hybridization effect and $s,p \rightarrow d$ electron transfer play an important role in promoting superconductivity at high pressures.

(iv) We also observe that superconductivity is very sensitive to the structure as the superconductivity observed in the cubic L_{12} structure is completely lost for the hexagonal DO_{19} structure.

We believe from our calculations that if the value of $N(E_F)$ is larger in the stable structure than the hypothetical structures, then the system will undergo a martensitic transformation. Further studies are needed in this direction.

ACKNOWLEDGMENTS

The authors would like to thank the Department of Atomic Energy (DAE), India, for their financial support. P.R. is grateful to Dr. S. Sankaralingam for his critical reading of the manuscript and Dr. S. Mathi Jaya and G. Pari for their useful discussions. The authors are thankful to Dr. G. Subramonium, Institute of Mathematical Sciences, for his help in carrying out the TB LMTO calculations and also to Dr. R. V. Ramanujan, Metallurgy group, Bhabha Atomic Research Centre, for the interesting discussions we had, especially on phase stability studies.

[1]E. M. Schulson, Int. Met. Rev. **29**, 195 (1984).
[2]E. M. Schulson and J. A. Roy, Acta Metall. **26**, 29 (1978).
[3]E. M. Schulson and J. A. Roy, Acta Metall. **26**, 15 (1978).
[4]E. M. Schulson, Metall. Trans. A **9**, 527 (1978).
[5]M. E. Eberhart and D. D. Vvedensky, Phys. Rev. B **37**, 8488 (1988).
[6]V. Raman, P. Mukhopadhyay, and S. Banerjee, Mater. Sci. Eng. **36**, 105 (1978).
[7]T. Hong, T. J. Watson-Yang, X. Q. Guo, A. J. Freeman, and T. Oguchi, Phys. Rev. **43**, 1940 (1991).
[8]P. Vinet, J. Ferrante, J. R. Smith, and J. H. Rose, J. Phys. C **19**, L467 (1986); P. Vinet, J. H. Rose, J. Ferrante, and J. R. Smith, J. Phys. Condens. Matter **1**, 1941 (1988).
[9]Wang-Rong Yao, Luo Q-Guang, and Zhang Xiao, Phys. Status Solidi A **90**, 763 (1985).
[10]Y. Akahama, M. Kobayashi, and H. Kawamura, J. Phys. Soc. Jpn. **59**, 3843 (1990).
[11]F. S. Galasso, *Structure and Properties of Inorganic Solids* (Pergamon, New York, 1970), p. 165; W. B. Pearson, *A Handbook of Lattice Spacing and Structures of Metals and Alloys* (Pergamon, New York, 1958).
[12]O. K. Andersen, Phys. Rev. B **12**, 3060 (1975).
[13]H. L. Skriver, *The LMTO Method* (Springer-Verlag, Berlin, 1984).
[14]S. Mathi Jaya R. Jagadish, R. S. Rao, and R. Asokamani, Mod. Phys. Lett. B **6**, 103 (1992).
[15]S. Mathi Jaya, R. Jagadish, R. S. Rao, and R. Asokamani, Phys. Rev. B **43**, 13 274 (1991).
[16]von Barth and L. Hedin, J. Phys. C **5**, 1629 (1972).
[17]O. K. Andersen (unpublished).
[18]S. K. Bose, J. K. Kudrnovsky, I. I. Mazin, and O. K. Andersen, Phys. Rev. B **41**, 7988 (1990).
[19]R. Kuentzler and R. M. Waterstrat, Solid State Commun. **68**, 85 (1988).
[20]Pasturel, C. Colinet, and P. Hicter, Physica **132B**, 177 (1985).
[21]O. Jepsen, O. K. Andersen, and A. R. Mackintosh, Phys. Rev. B **12**, 3084 (1975).
[22]De-Cheng Tian and Xiao-Bing Wang, J. Phys. Condens. Matter **4**, 8765 (1992).
[23]R. Hoffmann, Rev. Mod. Phys. **60**, 601 (1988).
[24]C. D. Gellatt, Jr., A. R. Williams, and V. L. Moruzzi, Phys. Rev. B **27**, 2005 (1983).
[25]E. M. Schulson and R. B. Turner, Phys. Status Solidi A **50**, 83 (1978).
[26]J. H. N. Van Vucht, J. Less-Common Met. **11**, 308 (1966).
[27]W. R. Yao, Phys. Status Solidi A **94**, 445 (1986).
[28]J. H. N. Van Vucht and K. H. J. Buschow, J. Less-Common Met. **10**, 98 (1965).
[29]J. H. Xu and A. J. Freeman, Phys. Rev. B **41**, 12 553 (1990).
[30]J. H. Xu, T. Oguchi, and A. J. Freeman, Phys. Rev. B **35**, 6940 (1987).
[31]J. H. Xu and A. J. Freeman, Phys. Rev. B **40**, 11 927 (1989).
[32]R. Kuentzler and R. M. Waterstrat, Solid State Commun. **54**, 517 (1985).
[33]J. H. Xu and A. J. Freeman, Phys. Rev. B **40**, 11 927 (1989).
[34]P. Ravindran and R. Asokamani (unpublished).
[35]P. Descouts, B. Perrin, A. Dupanloup, and A. Treyvaud, J. Phys. Chem. Solids **39**, 161 (1978).
[36]C. W. Chu, E. Bucher, A. S. Cooper, and J. P. Maita, Phys. Rev. B **4**, 320 (1971).
[37]A. Oota, H. Kusunoki, M. Tsuchiga, H. Takei, and S. Noguchi, J. Phys. F **15**, 1103 (1985).
[38]K. A. Gschneidner, Solid State Phys. **16**, 309 (1964).
[39]W. L. McMillan, Phys. Rev. **167**, 331 (1968).
[40]R. Asokamani, M. Rajagopalan, M. B. Suvasini and V. Sundararajan, Phys. Rev. B **33**, 7556 (1986).
[41]H. L. Skriver and I. Mertig, Phys. Rev. B **32**, 4431 (1985).
[42]D. A. Papaconstantopoulos, L. L. Boyer, B. H. Klein, A. R. Williams, and J. F. Janak, Phys. Rev. B **15**, 4221 (1977).
[43]K. A. Gschneidner, Solid State Phys. **16**, 371 (1964).
[44]R. Asokamani, G. Subramoniam, S. Mathi Jaya, and S. Pauline, Phys. Rev. B **44**, 2283 (1991).
[45]N. V. Zavaritskii, E. S. Itskevich, and A. N. Voronovskii, Zh. Eksp. Teor. Fiz. **60**, 1408 (1971) [Sov. Phys. JETP **33**, 762

(1971)].
[46]R. J. Kematick, H. F. Franzen, and K. Misemer, J. Solid State Chem. **60**, 97 (1985).
[47]P. Mukhopadhyay, V. Raman, S. Banerjee, and R. Krishnan, J. Mater. Sci. Lett. **23**, 2066 (1978).
[48]J. H. Xu and A. J. Freeman, Phys. Rev. B **41**, 12 553 (1990); J. Mater. Res. **6**, 1188 (1991).
[49]T. Nautial and S. Auluck, Phys. Rev. B **45**, 13 930 (1992).
[50]B. M. Klein, L. L. Boyer, and D. A. Papaconstantopoulous, Phys. Rev. Lett. **42**, 530 (1979).
[51]R. Asokamani, G. Subramoniam, S. Pauline, and R. Umamaheswari (unpublished).
[52]A. K. McMahan, Physica B **139&140B**, 31 (1986).
[53]K. Syassen *et al.*, in *Physics of Solids Under High Pressure,* edited by J. S. Schilling and R. N. Shelton (North-Holland, Amsterdam, 1981), p. 125.
[54]W. H. Butler, in *Treatise on Materials Science and Technology,* edited by Frank Y. Fradin (Academic, New York, 1981), Vol. 21, pp. 165–221; W. H. Butler, Phys. Rev. B **15**, 5267 (1977).
[55]R. Asokamani, M. B. Suvasini, M. Rajagopalan, and V. Sundararajan, Physica B **138**, 94 (1986).
[56]C. G. Jiang, G. Fletcher, J. L. Fry, and D. A. Papaconstantopoulous, Phys. Rev. B **44**, 2268 (1991).
[57]R. Asokamani and K. Iyakutti, J. Phys. **10**, 1157 (1980).
[58]M. Raychaudhury, P. Chatterjee, and S. Chatterjee, Phys. Status Solidi B **90**, 609 (1978).